Onset of grain motion in eroding subaqueous bimodal granular beds

Marios Galanis,[1] Philip Wang,[2] Mark D. Shattuck,[3]
Corey S. O'Hern,[2,4,5] and Nicholas T. Ouellette[1,*]

[1]*Department of Civil and Environmental Engineering, Stanford University, Stanford, California 94305, USA*
[2]*Department of Mechanical Engineering and Materials Science, Yale University, New Haven, Connecticut 06520, USA*
[3]*Benjamin Levich Institute and Physics Department, The City College of the City University of New York, New York, New York 10031, USA*
[4]*Department of Applied Physics, Yale University, New Haven, Connecticut 06520, USA*
[5]*Department of Physics, Yale University, New Haven, Connecticut 06520, USA*

(Received 21 January 2021; accepted 25 August 2021; published 7 September 2021)

We report experimental measurements of the onset of grain motion in fully submerged erodible beds containing grains of two sizes driven by a turbulent shear flow. Although we find that a traditional Shields-number framework successfully accounts for grain-size effects in beds composed of grains of only a single size, our results show that bimodal beds are distinct in a way that cannot be captured by a Shields-number rescaling. In particular, we find that large grains in a bimodal bed are mobilized into bedload transport by stresses that would normally be subcritical for them but that the behavior of small grains is less significantly affected. By analyzing higher-order statistics, we reveal the key role played by the granular contact and force networks in the bed near onset and clarify the impact of grain-size polydispersity on the transition from a static to an eroding bed. Our results have implications for modeling sediment transport in natural systems where polydispersity is unavoidable.

DOI: 10.1103/PhysRevFluids.6.094301

I. INTRODUCTION

Erosion and weathering of earth materials play key roles in shaping landscapes over a wide range of timescales [1]. One environmentally common and important example of this broad class of geophysical phenomena is the mobilization of submerged sediments by shear flows, such as in riverine systems [2]. Understanding sediment transport in principle requires both granular physics, to describe the properties of the sediment bed, and fluid mechanics, to describe how the fluid flow generates hydrodynamic stresses and transmits them to the bed. Thus the dominant paradigm for nearly a century has been to try to describe sediment transport near the onset of grain motion in an erodible bed driven by a shear flow in terms of a nondimensional parameter known as the Shields number that compares the hydrodynamic stress delivered to the bed to the weight of a bed grain.

Beginning with the pioneering work of Shields [3], data from field observations, laboratory experiments, and numerical simulations have been compiled to produce an empirical relationship, known as the Shields curve, that attempts to specify a critical Shields number as a function of the flow Reynolds number above which bed grains will be mobilized [4]. Although theoretical arguments have been proposed to explain the shape of the Shields curve [5–7], it still remains largely empirical. The data that go into determining the Shields curve also persistently display

*nto@stanford.edu

significant scatter [4], suggesting that this simple framework for understanding the onset of grain motion is likely incomplete. In particular, it averages over both the complex physics of turbulent flow and granular mechanics, incorporating turbulence only through a Reynolds number and granular physics only through the grain weight. Thus, the Shields-curve framework largely neglects turbulent fluctuations [8,9] and the long-range, nonlocal force correlations that are possible and common in granular packings [10,11].

One aspect that is likely to play a role in the stability of the bed but whose importance is not settled is grain-size polydispersity [12–14]. The simplest way to treat polydispersity is simply to average over the grain-size distribution and consider the bed as if it were uniformly composed of grains of a "typical" size such as the median diameter [4]. This approach is very simple and does not require detailed knowledge of the grains. However, it may not correctly predict sediment transport rates without the use of empirical correction factors [15,16] and cannot account for grain sorting processes that may occur during flow [12,15]. More complex proposals recognize both that different grain sizes may respond to the driving flow differently and that the presence of multiple grain sizes may change the stability of any particular grain size relative to a monodisperse bed. To account for these effects, the grain-size distribution is discretized, and grains in different size classes are considered separately. Relative size effects are modeled via so-called "hiding functions" [12,17,18]. However, such models are largely empirical and rely on fits to data rather than arising from first-principles theory. In particular, they do not explicitly account for how the details of the grain contact (and therefore force) networks may be modified in polydisperse beds [19].

Here, to gain more insight into the impacts of grain-size polydispersity near the onset of motion in erodible beds, we experimentally study the simplest case of a bimodal bed (that is, a bed containing grains of two sizes) driven by an overlying turbulent shear flow. We compare our results for bimodal beds with experiments on unimodal beds using the same experimental protocols and measurement techniques. We find that for unimodal beds, as expected, defining an appropriate grain-size-specific Shields number and choosing a proper velocity scaling allows us to collapse the onset curves for both small and large grains. However, we find that this approach does not work when considering the behavior of large and small grains separately in bimodal beds. To probe these results more deeply, we then perform a more detailed statistical analysis to show that bimodal beds are fundamentally different from unimodal beds. Our results indicate that, particularly for the case of bimodal beds, the physics of granular packings cannot be ignored in characterizing the strength and failure of the bed. This finding in turn has implications for modeling the onset of erosion in real beds, which are always polydisperse, and suggests connections with bed armoring [20–22].

We begin in Sec. II below by describing our experimental protocols and data acquisition system, including the flow apparatus and the way we prepare the granular beds. In Sec. III we present the results, beginning with average grain behavior in unimodal and bimodal beds. We then calculate higher-order statistics that probe the complexity of this system. Finally, in Sec. IV we summarize and contextualize our findings.

II. EXPERIMENTAL METHODS

The experimental apparatus, protocols, and measurement techniques are similar to what we have reported previously in a study of the onset of grain motion in monodisperse granular beds [9]. Here we therefore give only a brief overview of the experiment.

A. Apparatus

Our experiments are conducted in a closed, racetrack-shaped channel consisting of two straight sections joined by U-shaped bends. The channel has a width of 5.08 cm and a full height of 21.25 cm. One of the straight sections is the test section where measurements are taken and is constructed with glass sidewalls and an acrylic top plate for optical access so that the granular bed and fluid flow can be imaged from the sides or the top. The test section contains the granular bed,

which is partially confined by two triangular wedges of height 5 cm fixed to the channel floor. These wedges prevent large-scale migration of the bed, so that most of the grains remain in the test section, and delay the formation of large-scale bedforms, allowing us to run our experiments for longer durations. In these experiments, we also inserted an acrylic plate 2 cm in height below the granular bed to reduce the total bed depth and therefore the required mass of grains in each experiment; even with this plate, however, the bed was always at least 25 grain diameters deep.

Flow in the channel is driven by a toothed belt connected to an external motor and mounted at the top of the apparatus in the middle of the other straight section, similar to a plane Couette flow. The belt drive is completely immersed in water, and the entire apparatus is sealed (and so has no free surface) to avoid entraining air into the water. The bulk flow velocity is set by controlling the motor speed and is monitored via a Pitot tube mounted at the downstream end of the test section. The Pitot tube is calibrated against detailed velocimetry conducted in the test section, as described below.

B. Flow characterization

To measure and quantify the fluid flow precisely, we used particle tracking velocimetry (PTV). We seeded the fluid with neutrally buoyant fluorescent polyethylene microspheres with a diameter of approximately 50 μm that behaved as flow tracers. We passed a vertical laser sheet, created using a 532 nm Nd:YAG laser and a cylindrical lens mounted above the apparatus, through the centerline of the test section, with the thin direction of the sheet in the spanwise direction. The tracer particles fluoresced when they passed through the laser sheet, and we imaged their motion with a 1-megapixel Photron Fastcam SA5 camera looking through the sidewall of the channel at a frame rate of 2000 frames per second. We recorded multiple brief 5-s videos and tracked the motion of the tracer particles using a predictive multiframe tracking algorithm [23]. From the particle trajectories, we computed accurate velocities by convolution with a smoothing and differentiating kernel [24]. Empirically, we found that the measured velocities were statistically repeatable for a given motor speed, allowing us both to establish a calibration between the reading of the Pitot tube and the detailed flow velocity and to measure spatially well resolved velocities by averaging over time. This averaging also allowed us to conduct the PTV with the sediment bed present to ensure that the flow properties were calibrated with the appropriate boundary conditions to reflect the experimental runs. Because our experiments were limited to flows below or just above the onset of sediment motion and we only measured the flow in a thin light sheet in the center of the channel, the number of moving sediment grains potentially observable during PTV was statistically negligible compared with the number of tracer particles. Thus, during experimental runs measuring the dynamics of the granular bed, it was not necessary to conduct PTV simultaneously.

Estimating the hydrodynamic stress applied to the granular bed requires a well-resolved vertical velocity profile. To construct a profile, we first bin the measured velocities of tracer particles based on their vertical position into bins 2 mm in height, ensuring that each bin contains at least 20 000 samples. We then carefully fit the profile using the method described by Rodríguez-López *et al.* [25], which allows us to extract the wall shear stress τ_w and the friction velocity $u_* = \sqrt{\tau_w/\rho_f}$, where ρ_f is the density of water. Examples of the measured velocity profiles and fits are shown in Fig. 1 for five different flow rates. Using τ_w, we can then compute the Shields number for each grain size i as

$$\Theta_i = \frac{\tau_w}{(\rho_g - \rho_f)gD_i}, \tag{1}$$

where ρ_g is the grain density, g is the acceleration due to gravity, and D_i is the diameter of grain i. Because the grain weight and therefore the denominator of the Shields number is fixed by our choice of materials, the Shields number and Reynolds number co-vary. In our experiments, the friction Reynolds number $\mathrm{Re}_\tau = u_*\delta/\nu$, where δ is the half-height of the channel in the test section and ν is the kinematic viscosity of water, ranges from 850 to 1340, and the shear Reynolds number

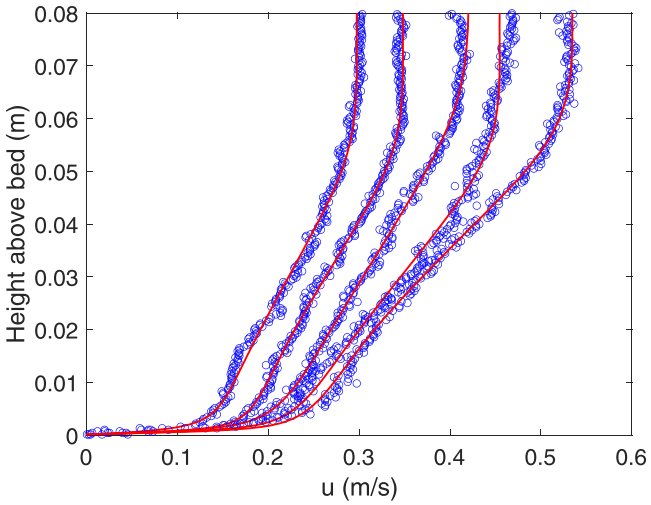

FIG. 1. Velocity profiles as measured from PTV for five representative flow rates. The solid lines are fits to the data using the method described by Rodríguez-López *et al.* [25], from which we extract the friction velocity and wall shear stress.

at the grain scale $\mathrm{Re}_* = u_* D_i/\nu$ ranges from 3.7 to 5.9 for the small grains and from 8.7 to 13.8 for the large grains.

C. Granular bed

The erodible bed is composed of soda lime glass beads with a mass density of $\rho_g = 2.5$ g/cm^3. For these experiments, we used beads of two different sizes: small beads with a diameter of $D_s = 0.375 \pm 0.125$ mm and large beads with a diameter of $D_\ell = 0.875 \pm 0.125$ mm. During the experiments, we illuminated the bed with two 300-W halogen lights and imaged its dynamics with a FLIR Grasshopper 3 color camera mounted above the apparatus and looking vertically down through the acrylic top plate. We captured images measuring 992×920 pixels with a spatial resolution of 37 μm per pixel at a rate of 250 frames per second. The camera was placed far enough from the entrance of the test section so that secondary flow effects from the bends and the beginning of the granular bed will have decayed.

Distinguishing the two different types of grains via their apparent size in the camera images is unreliable. Thus we used grains of different colors instead: the small grains were colored gold, and the large grains were blue. Even with this difference in color, however, we found that attempting to separate the grains in the typical red-green-blue (RGB) color space output natively by our camera was nonideal, because the color channels bleed into one another and stray reflections were difficult to distinguish from grains. Instead, we obtained much more reliable results by transforming the images into the hue-saturation-value (HSV) color space. To segment the raw images into images of blue grains and images of gold grains, we ran a k-means clustering algorithm (assuming $k = 2$) on the H component of the images. Finally, to obtain the positions of individual grains in these segmented images accurately, we used a circular Hough transform. After obtaining grain positions in each frame, we tracked the grain motion using the same predictive tracking algorithm that we used for the flow PTV to obtain time-resolved grain trajectories.

Because this image segmentation procedure worked very well, we also used it for the unimodal beds. These beds were composed of grains of all the same size but again two different colors, in an 80/20 mixture by volume. Working with only the color occupying 20% of the volume made

imaging and tracking much easier and more reliable while still allowing us to collect statistics efficiently, similar to what has been reported previously in similar experiments [9,12,26].

D. Experimental protocol

The first step in running an experiment is the preparation of the granular bed. For bimodal beds, we mixed together equal volumes of each grain size (so that the volume fraction of each size is 50%); for unimodal beds, we mixed grains of the same size but of two different colors (as described above) in an 80/20 mixture by volume. The total mass of grains was kept the same for all cases. To ensure a reasonably homogeneous mixture of the two grain sizes, we first stirred the beads gently in a container until they were well mixed and then poured them into the test section of the channel to a depth of roughly 2.25 cm. Because the size difference between the two types of grains was not too large, size segregation via kinetic sieving was not a strong effect. Although the beds prepared in this way were unlikely to be perfectly homogeneous, they were sufficiently mixed so that averaging the results over several trials in independently prepared beds should suppress any effects of residual inhomogeneity. The apparatus was then filled with water, and the bed was subjected to a slow flow, well below the threshold of grain motion, to flush trapped air in the system. This treatment also settled grains that were originally located in very unstable positions into more natural configurations.

Once the bed was prepared, we increased the flow velocity quasistatically in small increments (of 6 cm/s). After each increase the system was allowed to stabilize for 45 s, after which a movie of the bed was captured. After data acquisition, the motor was reversed and a flow in the opposite direction above the threshold for grain motion was briefly applied to destroy any armoring that may have taken place during data acquisition [27]. The motor was then set to run in its forward direction again, the velocity was incremented, and another set of data was acquired. This procedure continued until the maximum desired flow velocity was reached. We consider here only flows near the onset of bed motion, and do not approach, for example, the transition to suspended-load transport. We also avoided flow-driven vertical size segregation by staying near the onset of motion.

III. RESULTS

A. Unimodal beds

We begin by considering the onset of erosion in unimodal beds composed of only small or large grains. We would expect that the average behavior of the two different cases should be largely similar (and consistent with the Shields curve) when scaled appropriately with a Shields number Θ_i computed using the corresponding grain size and a properly nondimensionalized velocity. The critical Shields number describing the onset of erosion is often taken to be the Shields number at which the net downstream grain flux becomes nonzero [4,26]. Rather than computing the grain flux per se, we instead measure the mean grain velocity $\langle u_g \rangle$ averaged over all identified grains as a proxy, as it should be proportional to the flux [9]. Note that this calculation includes identified grains that are not moving in the averaging and so will be lower than the typical velocity of the moving grains.

In Fig. 2(a) we show the dimensional mean grain velocity as a function of the wall shear stress for the two unimodal beds. As expected, for small stresses the mean grain velocity is zero, indicating a static bed. Above a critical stress the mean grain velocity begins to rise as individual grains begin to move in bedload transport. As expected, this critical stress is clearly larger for the large grains than it is for the small grains, so that at any given stress above onset, small grains are moving faster than large grains. To compare the two data sets dynamically, we must nondimensionalize both axes. We first scale the wall shear stress by the grain weight to compute a grain-specific Shields number Θ_i as given by Eq. (1). However, we must also account for the variation of the critical Shields number with the grain-scale Reynolds number [4,7]. As we have described previously [9], pinpointing a precise critical Shields number $\Theta_{i,c}$ is difficult, particularly for the turbulent flows we consider here. However, we can estimate $\Theta_{i,c}$ for each grain size from the onset curves shown in Fig. 2(a),

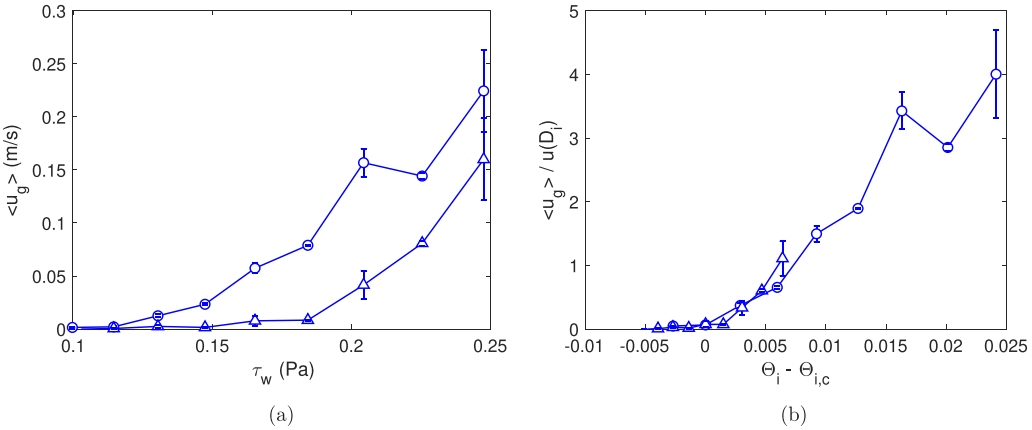

FIG. 2. (a) Mean grain velocity $\langle u_g \rangle$ averaged over all identified grains in unimodal beds plotted as a function of the bed shear stress τ_w for small grains (circles) and large grains (triangles). Error bars show the standard error computed over six trials. (b) The same data as in (a) but scaled by the flow velocity evaluated one grain diameter above the bed $u(D_i)$ and plotted as a function of $\Theta_i - \Theta_{i,c}$, where Θ_i is the grain-specific Shields number and $\Theta_{i,c}$ is the estimated critical Shields number.

obtaining results that are consistent both with our previous results [9] and with models [5] and other compiled measurements [4,7].

It is less obvious how best to scale the velocity. The Stokes settling velocity $V_S = \sqrt{gD_i(\rho_g - \rho_f)/\rho_f}$ is sometimes used [26], as it scales with the grain size. However, the settling velocity is a characteristic scale in the vertical direction and thus should not be expected to capture the speed of grains in bedload transport that are always in contact with the bed and so are not settling. A typical streamwise velocity scale is the friction velocity u_*, but it does not account for grain size. We therefore choose to scale the mean grain velocity by $u(D_i)$, the mean flow velocity (as measured from our PTV) evaluated one grain diameter above the bed, as this captures both the typical downstream speed and varies with grain size.

In Fig. 2(b) we show the same data as in Fig. 2(a) but now scaled as described here. As desired, the two onset curves collapse well, indicating that these scalings are appropriate and that (as expected) grain-size effects can be scaled out of the typical bed dynamics.

B. Bimodal beds

This situation may change when we consider in detail the behavior of bimodal beds containing grains of both sizes. Real erodible beds in natural systems are of course always polydisperse [17] but are often treated as being composed of some representative grain size such as the mean or mode of the size distribution [4,20]. Here, because we are able to identify the small and large grains separately, we can consider their behavior independently even when they are both in the apparatus at the same time. We can thus investigate how their individual dynamics are altered due to the presence of the other grain size.

In Fig. 3 we compare the mean grain speed as a function of the grain-specific Shields number for grains in unimodal beds and for small and large grains in bimodal beds considered separately. As in the previous section, we scale the mean grain velocity by the mean flow velocity evaluated one grain diameter above the bed; however, we do not remove a critical Shields number, because we plot onset curves for small and large grains separately. When plotted in this way, the onset curves for small grains in unimodal and bimodal beds collapse; the presence of the large grains does not appear to affect their onset behavior. The large grains are quite different, however. Large grains in bimodal beds both begin to move at a lower critical Shields number than in unimodal beds and have

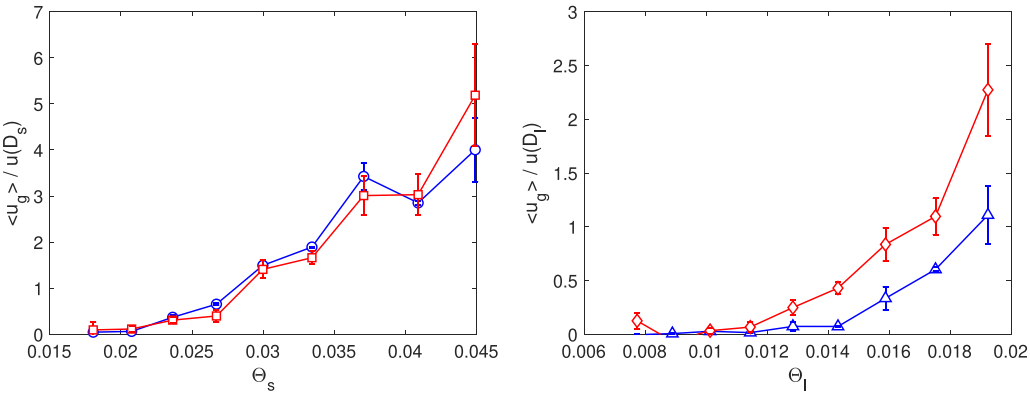

FIG. 3. Comparison of the mean grain velocity $\langle u_g \rangle$ in unimodal beds (blue circles and triangles) and bimodal beds (red squares and diamonds) for (a) small grains and (b) large grains. The unimodal data are the same as in Fig. 2(b). For the bimodal data, $\langle u_g \rangle$ is computed by averaging over all identified grains of a particular size, and the error bars show the standard error computed over 11 trials. Grain velocities are scaled by the mean flow velocity evaluated at one grain diameter above the bed as in Fig. 2(b), and data are plotted as a function of the small- and large-grain Shields numbers Θ_s and Θ_l, respectively. Data for small grains in unimodal and bimodal beds (a) collapse when plotted in this way, but the same is not true for the large grains.

a higher mean velocity. A potential explanation for this observation is that once the small grains start moving in a bimodal bed, they destabilize the granular packing, which then allows the large grains to move; we will return to this conjecture in the following section. Our results also indicate that Θ_i is not the only parameter that controls the onset of grain motion in bimodal beds.

In polydisperse beds, a Shields number based on an average or composite grain size is sometimes used [4] to try to account for the size variation. However, since the small grains appear to behave identically in unimodal and bimodal beds but the large grains do not, no single choice for a Shields number in bimodal beds could reconcile our data. Thus, our results indicate that the traditional Shields framework is not sufficient to capture the details of the onset of erosion in polydisperse beds and that additional physics beyond fluid mechanics may need to be included. Given the conjecture in the previous paragraph that the entrainment of small grains in bimodal beds at stresses that would ordinarily be subcritical for large grains may destabilize the large grains, we suggest that this missing physics lies in the granular contact and stress networks.

C. Higher-order statistics

Studying the average grain speed does not give a complete picture of the bed dynamics near the onset of motion; as with most systems involving turbulent flow, higher-order statistics are highly nontrivial and must be considered to understand the physics. We thus consider now not just averages but rather the full probability density functions (PDFs) of the grain velocities. In our previous work [9] we studied these PDFs near the onset of net grain motion for the case of unimodal beds and showed that they have a central core that reflects the turbulent fluctuations and a long tail that characterizes mobilized grains. Here we extend this work for the case of bimodal beds.

In Fig. 4 we show PDFs of the instantaneous grain velocities for the case of small grains in a bimodal bed for five different Shields numbers. To create these PDFs, we included the velocities measured for each tracked grain, which primarily lay on the top of the bed. Note that the number of samples used to create each PDF was not the same, since we cannot control the number of detected grains. The number of samples was, however, comparable in each case, regardless of how fast the grains were moving. The grain velocity PDFs have the same qualitative shape as what we reported

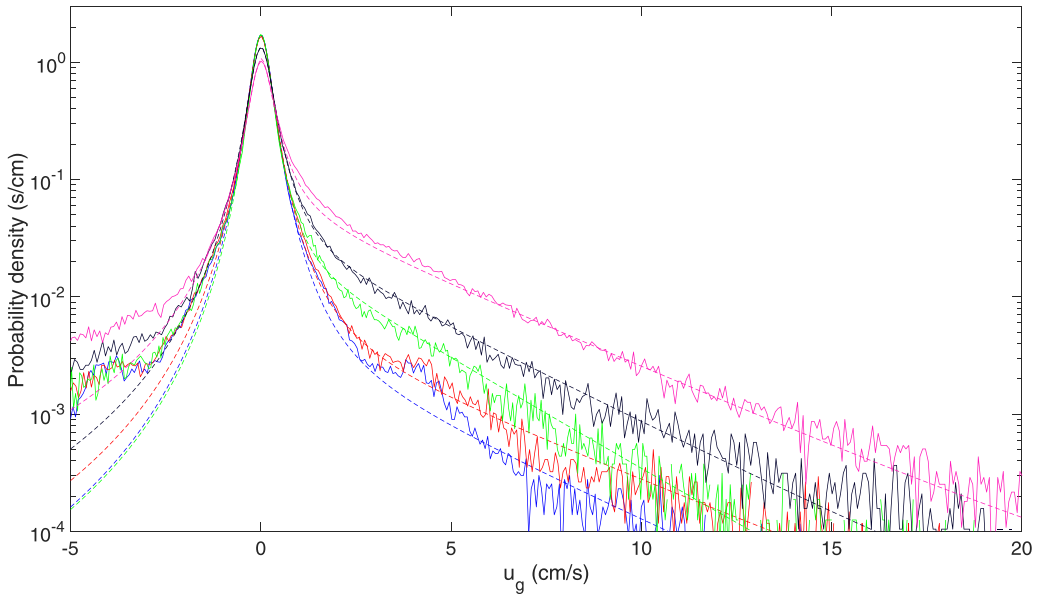

FIG. 4. Representative velocity probability density functions (PDFs) for the case of small grains in bimodal beds (solid lines); results for other experimental cases are qualitatively similar. Data are shown for $\Theta_s = 0.018$, 0.024, 0.030, 0.037, and 0.045, from bottom to top. The dashed lines are fits of Eq. (2).

before for unimodal beds [9]; thus the qualitative interpretation of these PDFs is not changed by the addition of a second grain size. This result also indicates that we can model the PDF in the same way as we did before. The central core of the PDF contains both positive and negative velocity fluctuations; these are related to in-place jitter of grains due to the turbulent fluctuations in the flow velocity and stress. Given the typical behavior of turbulence statistics, one would not expect these fluctuations to be entirely Gaussian. Turbulence theory, however, cannot directly predict their shape, since the grains will filter the turbulent fluctuations due to their finite size and mass relative to the fluid [28,29]. Instead, we model this core region of the PDFs phenomenologically with a student's t distribution, which allows us to capture both the positive and negative fluctuations and the heavier-than-Gaussian tails. For larger Shields numbers, the PDFs also display a long, nearly exponential tail in the downstream velocity fluctuations. This part of the PDFs is associated with stochastic and independent mobilization of individual grains [30,31]. We model this tail with an exponential distribution. The entire PDF can then be fit by a linear mixture model of these two distributions given by

$$P(u_g) = A\frac{\Gamma\left(\frac{\zeta+1}{2}\right)}{\sigma\sqrt{\zeta\pi}\,\Gamma\left(\frac{\zeta}{2}\right)}\left[\frac{\zeta + \left(\frac{u_g}{\sigma}\right)^2}{\zeta}\right]^{\left(-\frac{\zeta+1}{2}\right)} + B\frac{1}{u_g^*}e^{-u_g/u_g^*}. \tag{2}$$

In this expression, A and B (which sum to unity) are the relative fractions of the t distribution and the exponential function in the mixture model. Γ is the Gamma function. σ sets the width of the t distribution, which characterizes the typical size of the velocity fluctuations. ζ is the shape parameter of the t distribution, which controls the heaviness of the tails; as $\zeta \to \infty$, the t distribution approaches a Gaussian. Finally, u_g^*, the relaxation constant of the exponential tail, sets a characteristic velocity scale for the mobilized grains only (and so should be expected to be larger than the mean grain velocity averaged over all detected grains $\langle u_g \rangle$ reported above) [9]. Fits of this model to the data are shown with the dashed lines in Fig. 4.

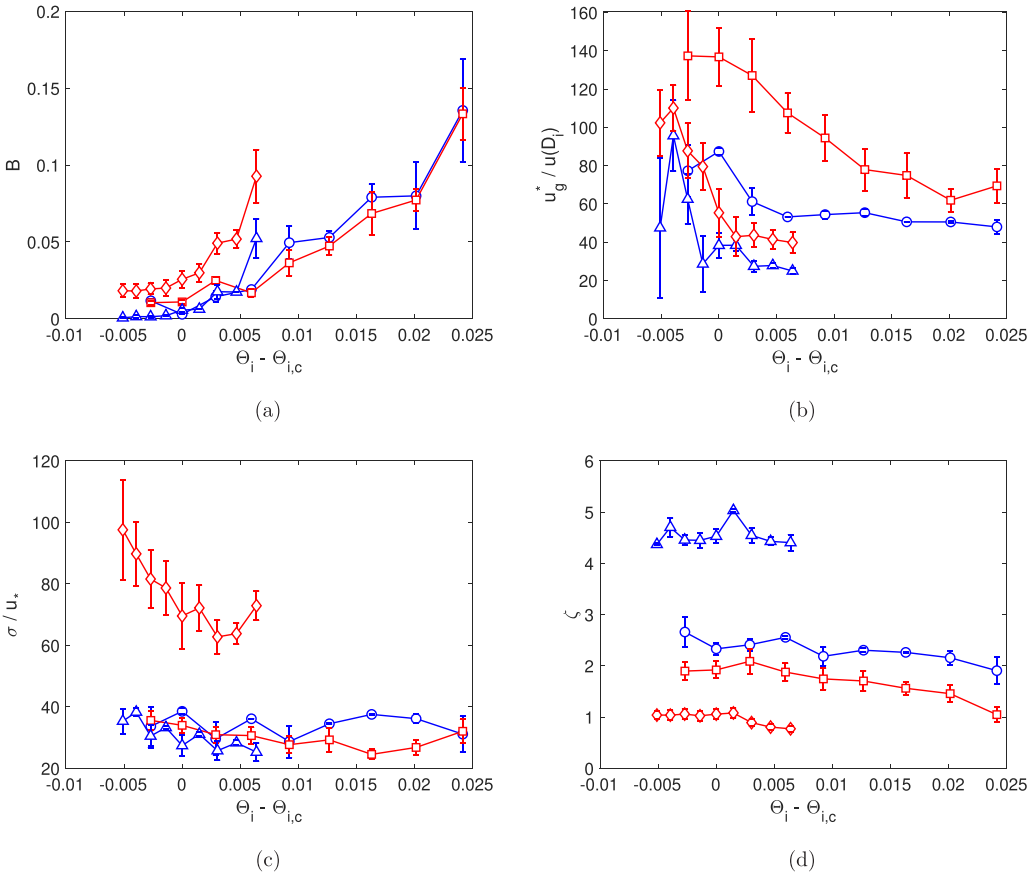

FIG. 5. Independent parameters in our model velocity PDF (that is, B, u_g^*, σ, and ζ) as determined from fits to the data for the four experimental cases considered as a function of the difference between the grain-specific Shields number Θ_i and the corresponding estimated critical value $\Theta_{i,c}$. Data are shown for small grains in unimodal beds (circles), small grains in bimodal beds (squares), large grains in unimodal beds (triangles), and large grains in bimodal beds (diamonds). The error bars represent standard errors, computed in the same way as in Figs. 2 and 3. The parameters B and ζ are dimensionless by construction. The typical speed of a moving grain u_g^* is scaled by the flow velocity one grain diameter above the bed $u(D_i)$, as above, and the typical velocity fluctuation σ is scaled by the friction velocity u_*.

We find that this mixture model fits well to all four experimental cases we considered over all Shields numbers. We can then compare the parameters from these PDFs to gain more insight into the differences between the behavior of unimodal and bimodal beds. In Fig. 5 we show the parameters B, u_g^*, σ, and ζ as functions of the grain-specific Shields number Θ_i for all of our data sets. The first two of these parameters (B and u_g^*) primarily give us information about the mobilized grains, while the second two (σ and ζ) are more reflective of the behavior of the grains that are not traveling downstream but rather are fluctuating in place.

B tells us the relative fraction of grains that are mobilized and not simply jittering in place due to turbulent fluctuations that are sufficient to make them move slightly but not strong enough to dislodge them from their pockets on the bed surface. The data in Fig. 5(a) show that, as one would expect, as the Shields number increases, the fraction of mobilized grains increases for all cases. However, the fraction of large grains mobilized at a given Shields number in bimodal beds is consistently higher than for all other cases. This result is consistent with the conjecture proposed in

the previous section that the presence of small grains destabilizes the large grains so that bimodal beds are inherently different from unimodal beds. Although there are many mechanisms by which this behavior could occur, two broad classes can be identified: entrained small grains can promote the mobilization of large grains either by increasing the stress delivered to them (via collisions) or by altering the local configuration around large grains, making them easier to dislodge.

We can distinguish these scenarios to a degree by investigating the typical speed of mobilized grains as characterized by u_g^* (scaled again by the mean flow velocity evaluated one grain diameter above the bed), shown in Fig. 5(b). As we have explained previously [9], below the onset of net grain motion at roughly $\Theta_{i,c}$, fitted values of u_g^* are unstable and have little meaning. Above the onset of grain motion, however, we can interpret the data. For large grains in both unimodal and bimodal beds and for small grains in unimodal beds, $u_g^*/u(D_i)$ is nearly constant once grains are mobilized. For small grains in bimodal beds, $u_g^*/u(D_s)$ decreases as the Shields number increases, approaching the result for small grains in unimodal beds at larger Shields number. The larger velocities near onset may be due to the presence of large grains on the surface, forcing a small grain moving in bedload transport in a bimodal bed to be higher in the water column than in a unimodal bed. Farther from onset, however, as grains begin to bounce higher off of the bed, this effect is diminished. Large grains in bimodal beds are similarly faster than large grains in unimodal beds, perhaps also due to enhanced heterogeneity and roughness of a bimodal bed [13]. We note that these results appear to be different from what was reported by Houssais and Lajeunesse [12] in a similar experiment, who found that the typical velocity of grains was not sensitive to the composition of the bed (though note that the way that typical velocities are defined is different between their analysis and ours).

To complete our discussion of the statistical properties of the grains, we also consider the two parameters (σ and ζ) that primarily contain information about the grains that are not experiencing net downstream movement, although they may still be fluctuating about their rest positions. In Fig. 5(c) we show σ, which captures the size of the typical velocity fluctuations of a nonmobile grain. Because we expect σ primarily to reflect fluctuations driven by the turbulence, we nondimensionalize it simply by the friction velocity u_*. The data clearly show that large grains in bimodal beds have a much larger σ than the three other cases, which are all comparable. This behavior can be interpreted consistently with the picture we have described above. In bimodal beds, small grains are more easily eroded than large grains. But as these small grains are removed from the bed surface, new pockets around the large grains open up, allowing the large grains to fluctuate more significantly without actually being eroded themselves. In contrast, small grains in bimodal beds that would have the same amount of freedom to fluctuate in place are simply entrained into the flow. The fluctuation behavior of unimodal beds is independent of the particle size, since eroding a particle and thus freeing up space on the bed surface functions in the same relative way when all the particles are the same size.

Finally, the behavior of the parameter ζ, shown in Fig. 5(d), tells a similar story. Recalling that larger values of ζ indicate fluctuations that are more nearly Gaussian, we see that unimodal beds are more Gaussian than bimodal beds. Large grains in unimodal beds are the closest to Gaussian of all of our four cases, since their larger inertia allows them to filter the turbulence more effectively [28,29]. In contrast, large grains in bimodal beds have the heaviest tails, since, as discussed above, they have the most space to fluctuate in place while still having enough inertia to be difficult to entrain into the flow.

IV. DISCUSSION AND CONCLUSIONS

We have reported the results of experiments driving turbulent shear flows over unimodal and bimodal granular beds. As expected, we found that data for the mean grain velocity as a function of the strength of the driving flow could be collapsed for unimodal beds using appropriate Shields numbers defined with the specific grain size and the flow velocity at a grain-specific height above the bed. However, a similar approach for collapsing the onset curves for small and large grains in bimodal beds was not successful. This result has important implications for the modeling of

sediment transport, as it suggests that large grains will be be mobilized even at subcritical shear stresses (relative to traditional critical Shields-number estimates). Finally, a deeper investigation of the higher-order statistics of the grain motion showed that the four experimental cases are all distinct from each other and revealed ways in which the granular physics of the bed and the turbulent fluctuations in the flow both play key roles in determining the dynamics of individual grains near the onset of bed motion.

At a high level, our results show that, near onset, unimodal and bimodal beds are fundamentally different in a way that cannot be captured by a simple Shields-number rescaling alone. This finding indicates that, as is not tremendously surprising given that it only coarsely considers the properties of the flow or the grains, the Shields-curve framework is incomplete. In our previous work [9], we showed how turbulent fluctuations contribute to the observed behavior near the onset of motion; here our results reveal how the detailed granular mechanics of the bed play an important role. The contact and force networks in unimodal and bimodal granular packings are unavoidably distinct [32], and the easy removal of some grains relative to others in bimodal beds can significantly alter the mechanical stability of the beds [20]. Future work on modeling the onset of sediment transport must take these granular effects into account.

Finally, we note that although it may be more obvious in polydisperse beds, the notion that some grains are easier to remove from a granular packing than others is not limited to the polydisperse case. Indeed, we have previously shown that the onset of motion in beds driven by shear flows tends to occur via the isolated failure of single "weak links" in the contact network [33,34]. As long as the system remains near onset so that these isolated failures do not compound and lead to a full mobilization of the bed, the annealing out of these weak points in the granular packing may be a mechanism leading to the gradual armoring and strengthening of the bed [20–22]. If so, this argument would suggest that grain-size polydispersity may significantly affect the armoring process, potentially leading to an enhanced capacity for armoring under some circumstances. This proposal would be interesting to test in future research.

ACKNOWLEDGMENTS

This research was sponsored by the Army Research Laboratory and was accomplished under Grant No. W911NF-17-1-0164 (M.G., P.W., C.S.O., and N.T.O.) The views and conclusions contained in this document are those of the authors and should not be interpreted as representing the official policies, either expressed or implied, of the Army Research Laboratory or the U.S. Government. We also acknowledge support from the National Science Foundation under Grant No. CBET-2002797 (M.D.S.).

[1] M. Houssais and D. J. Jerolmack, Toward a unifying constitutive relation for sediment transport across environments, Geomorphology **277**, 251 (2017).

[2] G. Seminara, Fluvial sedimentary patterns, Annu. Rev. Fluid Mech. **42**, 43 (2010).

[3] A. Shields, Anwendung der Ähnlichkeitsmechanik und der Turbulenzforschung auf die Geschiebebewegung, Ph.D. thesis, in *Mitteilungen der Preußischen Versuchsanstalt für Wasserbau und Schiffbau*, Vol. 26 (Preussischen Versuchsanstalt für Wasserbau, Berlin, 1936).

[4] J. M. Buffington and D. R. Montgomery, A systematic analysis of eight decades of incipient motion studies, with special reference to gravel-bedded rivers, Water Resour. Res. **33**, 1993 (1997).

[5] P. L. Wiberg and J. D. Smith, Calculations of the critical shear stress for motion of uniform and heterogeneous sediments, Water Resour. Res. **23**, 1471 (1987).

[6] C. H. Ling, Criteria for incipient motion of spherical sediment particles, J. Hydraul. Eng. **121**, 472 (1995).

[7] S. Dey, Sediment threshold, Appl. Math. Model. **23**, 399 (1999).

[8] P. Diplas, C. L. Dancey, A. O. Celik, M. Valyrakis, K. Greer, and T. Akar, The role of impulse on the initiation of particle movement under turbulent flow conditions, Science **322**, 717 (2008).

[9] J. C. Salevan, A. H. Clark, M. D. Shattuck, C. S. O'Hern, and N. T. Ouellette, Determining the onset of hydrodynamic erosion in turbulent flow, Phys. Rev. Fluids **2**, 114302 (2017).
[10] H. M. Jaeger, S. R. Nagel, and R. P. Behringer, Granular solids, liquids, and gases, Rev. Mod. Phys. **68**, 1259 (1996).
[11] J. Geng, D. Howell, E. Longhi, R. P. Behringer, G. Reydellet, L. Vanel, E. Clément, and S. Luding, Footprints in the Sand: The Response of a Granular Material to Local Perturbations, Phys. Rev. Lett. **87**, 035506 (2001).
[12] M. Houssais and E. Lajeunesse, Bedload transport of a bimodal sediment bed, J. Geophys. Res. Earth Surf. **117**, F04015 (2012).
[13] K. M. Hill, J. Gaffney, S. Baumgardner, P. Wilcock, and C. Paola, Experimental study of the effect of grain sizes in a bimodal mixture on bed slope, bed texture, and the transition to washload, Water Resour. Res. **53**, 923 (2017).
[14] F. Staudt, J. C. Mullarney, C. A. Pilditch, and K. Huhn, The role of grain-size ratio in the mobility of mixed granular beds, Geomorphology **278**, 314 (2017).
[15] R. P. Hunziker and M. N. R. Jaeggi, Grain sorting processes, J. Hydraul. Eng. **128**, 1060 (2002).
[16] M. Wong and G. Parker, Reanalysis and correction of bed-load relation of Meyer-Peter and Müller using their own database, J. Hydraul. Eng. **132**, 1159 (2006).
[17] H. A. Einstein, The bed-load function for sediment transportation in open channel flows, United States Department of Agriculture, Technical Bulletin No. 1026, 1950.
[18] J. W. Kirchner, W. E. Dietrich, F. Iseya, and H. Ikeda, The variability of critical shear stress, friction angle, and grain protrusion in water-worked sediments, Sedimentology **37**, 647 (1990).
[19] C. Voivret, F. Radjaï, J.-Y. Delenne, and M. S. El Youssoufi, Multiscale Force Networks in Highly Polydisperse Granular Media, Phys. Rev. Lett. **102**, 178001 (2009).
[20] C. O. Chin, B. W. Melville, and A. J. Raudkivi, Streambed armoring, J. Hydraul. Eng. **120**, 899 (1994).
[21] B. Ferdowsi, C. P. Ortiz, M. Houssais, and D. J. Jerolmack, River-bed armouring as a granular segregation phenomenon, Nat. Commun. **8**, 1363 (2017).
[22] B. Allen and A. Kudrolli, Granular bed consolidation, creep, and armoring under subcritical fluid flow, Phys. Rev. Fluids **3**, 074305 (2018).
[23] N. T. Ouellette, H. Xu, and E. Bodenschatz, A quantitative study of three-dimensional Lagrangian particle tracking algorithms, Exp. Fluids **40**, 301 (2006).
[24] N. Mordant, A. M. Crawford, and E. Bodenschatz, Experimental Lagrangian probability density function measurement, Physica D **193**, 245 (2004).
[25] E. Rodríguez-López, P. J. K. Bruce, and O. R. H. Buxton, A robust post-processing method to determine skin friction in turbulent boundary layers from the velocity profile, Exp. Fluids **56**, 6 (2015).
[26] E. Lajeunesse, L. Malverti, and F. Charru, Bed load transport in turbulent flow at the grain scale: Experiments and modeling, J. Geophys. Res. Earth Surf. **115**, F04001 (2010).
[27] C. C. Masteller, N. J. Finnegan, J. M. Turowski, E. M. Yager, and D. Rickenmann, History-dependent threshold for motion revealed by continuous bedload transport measurements in a steep mountain stream, Geophys. Res. Lett. **46**, 2583 (2019).
[28] A. Soldati, Particles turbulence interactions in boundary layers, Z. Angew. Math. Mech. **85**, 683 (2005).
[29] J. Bec, L. Biferale, G. Boffetta, A. Celani, M. Cencini, A. Lanotte, S. Musacchio, and F. Toschi, Acceleration statistics of heavy particles in turbulence, J. Fluid Mech. **550**, 349 (2006).
[30] J. C. Roseberry, M. W. Schmeeckle, and D. J. Furbish, A probabilistic description of the bed load sediment flux: 2. Particle activity and motions, J. Geophys. Res. Earth Surf. **117**, F03032 (2012).
[31] D. J. Furbish and M. W. Schmeeckle, A probabilistic derivation of the exponential-like distribution of bed load particle velocities, Water Resour. Res. **49**, 1537 (2013).
[32] J. F. Peters, M. Muthuswamy, J. Wibowo, and A. Tordesillas, Characterization of force chains in granular material, Phys. Rev. E **72**, 041307 (2005).
[33] A. H. Clark, M. D. Shattuck, N. T. Ouellette, and C. S. O'Hern, Onset and cessation of motion in hydrodynamically sheared granular beds, Phys. Rev. E **92**, 042202 (2015).
[34] A. H. Clark, M. D. Shattuck, N. T. Ouellette, and C. S. O'Hern, Role of grain dynamics in determining the onset of sediment transport, Phys. Rev. Fluids **2**, 034305 (2017).